

MODIFYING LAYERED DOUBLE HYDROXIDE NANOPARTICLES FOR TUMOR IMAGING AND THERAPY

LI LI¹, BEI LI¹, WENYI GU¹, AND ZHI PING XU^{1*}

¹Australian Institute for Bioengineering and Nanotechnology, The University of Queensland, Brisbane, QLD 4072, Australia

Abstract—Tumor theranostics (a portmanteau of therapeutics and diagnostics) is now achieved in various ways with complex nanoparticle systems. Layered double hydroxide (LDH) nanoparticles are effective at drug/gene delivery and as imaging agents in potential tumor theranostics. This mini-review paper summarizes recent progress in developing LDH nanoparticles as a pH-sensitive magnetic resonance imaging (MRI) contrast agent, as a positron emission tomography (PET) imaging agent, and as a co-delivery platform for two therapeutic agents for tumor diagnosis and therapy. These results have indicated clearly the potential application of LDH nanoparticles for simultaneous diagnosis and treatment of cancers.

Keywords—Co-delivery of Therapeutic Agents · Imaging Agent · Layered Double Hydroxide · MRI · PET · Tumor Theranostics

INTRODUCTION

Layered double hydroxides (LDH) are a group of anionic clay materials which have, in recent years, attracted increasing attention for biomedical applications such as disease imaging and delivery of genes, drugs, and vaccines for anti-cancer and anti-bacterial treatments (Choy et al., 2004; Xu et al. 2008a, 2008b; Choi & Choy, 2011). The LDH materials have several unique features, including large anionic exchange capacities, biocompatibility, facilitation of the cellular uptake of payloads, protection of payloads, and control-release of biomolecules and drugs in a pH-dependent manner (Li, L et al., 2015; Li X. et al., 2015). The inherent surface positive charge and anion exchange property enable LDH nanoparticles to carry and deliver anionic biomolecules and pharmaceutical drugs such as oligonucleotides (Li et al., 2014), DNAs (Desigaux et al., 2006), siRNAs (Chen, C. et al., 2013; Chen, M. et al. 2013; Wong et al., 2012), methotrexate (Choi et al., 2016), 5-fluorouracil (Li et al., 2014), and anti-inflammatory drugs (diclofenac, gemfibrozil, ibuprofen, and naproxen) (Khan et al. 2001).

As a natural mineral and readily synthesized material, LDH has a hydrotalcite-like structure, consisting of positively charged brucite-like cationic layers, negatively charged interlayer anions, and hydrogen-bonded water molecules, with a general composition formula of $[M^{2+}_{1-x}M^{3+}_x(\text{OH})_2]^{x+}(A^{n-})_{x/n} \cdot m\text{H}_2\text{O}$, where M^{2+} , M^{3+} , and A^{n-} represent divalent and trivalent metal cations and anions, respectively (Wang & O'Hare, 2012; Xu et al., 2008a, 2008b). Apart from the unique structure and properties which make for efficient delivery vehicles, many fluorescent dyes and inorganic nanoparticles have been tethered to LDH for optical imaging, X-ray computed tomography (CT), and magnetic resonance imaging (MRI) (Xu et al., 2008a, 2008b; Chen, M. et al., 2013; Chen, C. 2013; Li et al., 2013; Wang et al., 2013; Lee 2014).

A reliable method was developed to produce homogeneously dispersed MgAl-LDH nanoparticles, in aqueous suspension, which have a well-controlled size (50–300 nm) (Xu et al., 2006a, 2006b). As MgAl-LDH nanoparticles are very positively charged (zeta potential of 30–50 mV) (2006), negatively charged proteins (e.g. bovine serum albumin [BSA]) are adsorbed readily on the surface to prevent possible aggregation in physiological buffers or in an in vivo environment (Gu et al. 2015), unlike so-called (3-aminopropyl)triethoxysilane (APTES) coating strategies (Park et al. 2005; Li, S. et al., 2015; Li, X. et al., 2015). The approach to colloidal stabilization of LDH nanoparticles in media underpins the LDH-based application in vivo.

Recent engineering of LDH nanoparticles has increased the number of potential biomedical applications as reported here and elsewhere. Engineering of LDH nanoparticles involves two parts, as outlined in Fig. 1: the first is to substitute isomorphically the metal cation (Mg^{2+}) in the layers by another functional metal cation, such as Mn, for magnetic resonance imaging (MRI) (Li et al. 2017; Zuo et al., 2017) and ^{64}Cu for positron emission tomography (PET) imaging (Shi et al., 2015) (e.g. when studying tumors in mice). The second strategy is to co-load two or more therapeutic agents in the interlayer space and on the surface (e.g. 5-FU and siRNA) for co-delivery, which may produce a synergistic effect in the tumor treatment via two distinct apoptosis pathways (Chen et al. 2014; Li et al., 2014). Recent work has allowed LDH to be used for multimode imaging and synergetic therapy (Mei et al., 2018a, 2018b).

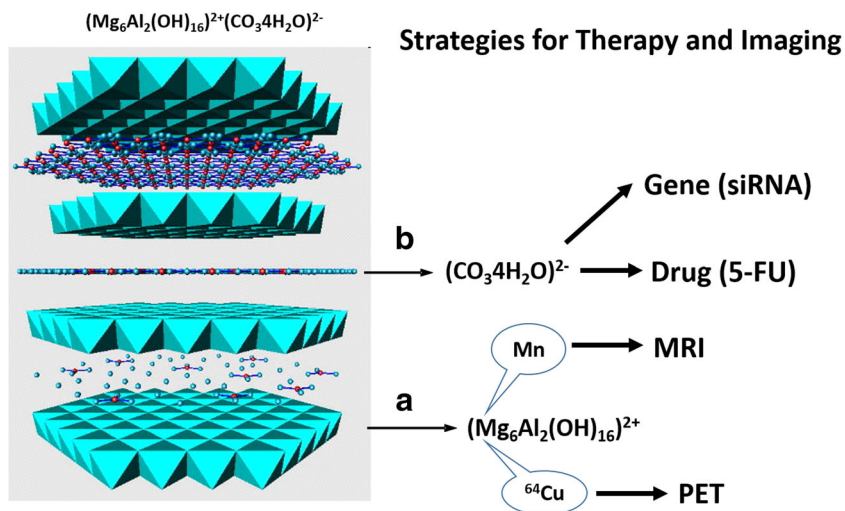
LDH-BASED IMAGING FOR TUMOR TISSUE

Replacement of Mg with Mn for MRI

Mn-containing MgAl-LDH (Mn-LDH) nanoparticles with ultrasensitive pH response and high relaxivity (the degree to which the agent can enhance the longitudinal or transverse water relaxation rate constant) have been developed and applied recently for MRI in this group. The synthesis of Mn-LDH nanoparticles was conducted first by co-precipitation (Xu et al., 2006a) to obtain a Mg_3Al -

* E-mail address of corresponding author: gordonxu@uq.edu.au
DOI: 10.1007/s42860-019-0006-z

Fig. 1 Strategies for tumor therapy and imaging based on MgAl-LDH physicochemical features: **a** Replacement of Mg with functional cations such as ^{64}Cu and Mn for tumor PET and MR imaging, respectively; **b** Intercalation or adsorption of therapeutic agents such as 5-fluorouracil (5-FU) and siRNA for combined tumor chemotherapy



LDH suspension and then by isomorphous substitution (Lee et al., 2014) of 0.8 of Mg^{2+} with Mn^{2+} ions ($\text{Mg}_{2.2}\text{Mn}_{0.8}\text{Al-LDH}$). As shown in Fig. 2a, as-prepared Mn-LDH nanoparticles had a plate-like morphology with lateral dimensions in the range 20–80 nm. Scanning transmission electron microscopy (STEM) (Fig. 2b) and elemental mapping images (Fig. 2c_{1–4}) display a uniform and homogeneous distribution of Mg, Al, Mn, and O within the particle, confirming the uniform substitution of Mn for Mg ions through the “dissolution-deposition-diffusion” process (Xu & Lu, 2005). X-ray photoelectron spectroscopy (XPS) revealed that >85% of Mn ions were divalent. Mn-LDH nanoparticles were, thus, obtained with Mn ions evenly dispersed on the hexagonal-like host layers, and the valence state of the Mn ions was mostly unchanged.

The in vitro T_1 -weighted relaxivity of Mn-LDH in buffer solutions (pH = 7.4, 7.0, 6.5, 6.0, and 5.0) was determined (Fig. 3a) to simulate the MRI capability of Mn-LDH NPs in normal body fluid (pH ≈ 7.4), in an acidic tumor microenvironment (pH ≈ 6.5–7.0), in the early endosome (pH ≈ 6.0), and in the late endosome/lysosome in cells (pH ≈ 5.0). Interestingly, the T_1 -weighted relaxivity (r_1) increased significantly by reducing the pH value of the aqueous solution from 7.4, via 7.0, 6.5, and 6.0, to 5.0, being 1.16, 6.82, 7.60, 8.24, and 9.48 $\text{mM}^{-1} \text{s}^{-1}$, respectively. This sharp change means that the relaxivity of Mn-LDH nanoparticles is very sensitive to the buffer pH around neutral condition. For example, the longitudinal relaxivity was increased by >6 times when the pH was changed from just 7.4 to 7.0 or 6.5. This ultrasensitivity to the environmental pH may be very useful in imaging

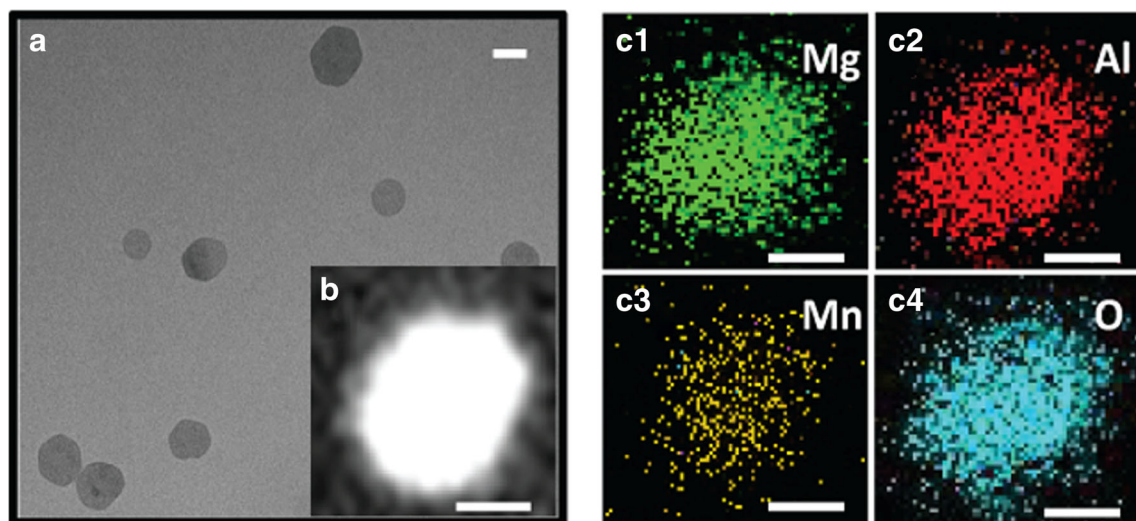
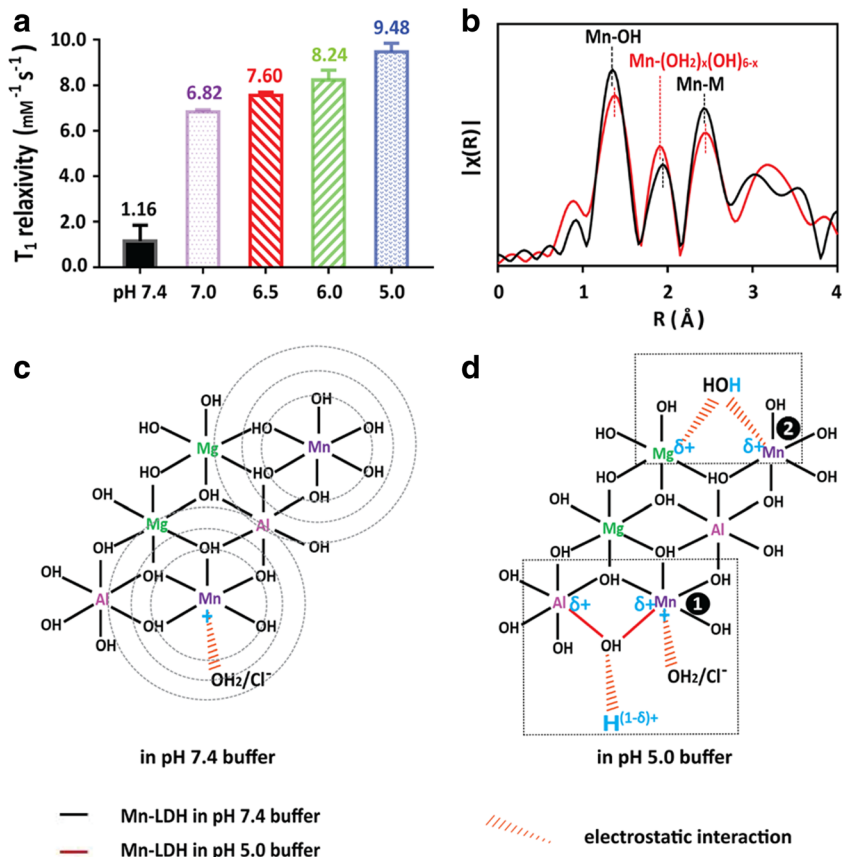


Fig. 2 a TEM image; b STEM image, and the corresponding element mapping of (c₁) Mg, (c₂) Al, (c₃) Mn, and (c₄) O of Mn-LDH nanoparticles. Scale bar: 20 nm. (Images reproduced with permission from Li et al. 2017)

Fig. 3 (a) Relaxivity (unit: $\text{mM}^{-1} \text{s}^{-1}$) of Mn-LDH nanoparticles after co-incubation in buffer solutions with various pH at 37°C for 4 h. Error bar = standard deviation, $n = 3$; (b) EXAFS spectra of Mn-LDH soaked in pH 7.4 and 5.0 buffers, respectively. Schematic structure changes of Mn-LDH nanoparticles in a pH = 7.4 buffer (c), and in a pH 5.0 buffer (d). (Images reproduced with permission from Li et al. 2017)



tumor tissues where the weak acidity can be used as the efficient ‘activatable’ factor. By comparison, the relaxivity of Mn-LDH nanoparticles in pH 7.0–5.0 buffers is 2–3 times greater than Gd-DTPA ($\sim 3.4 \text{ mM}^{-1} \text{ s}^{-1}$) (Donahue et al., 1994).

The large r_1 value of Mn-LDH nanoparticles in pH 5.0–7.0 buffers can be attributed to the peculiar microstructure of Mn(II) on the LDH surface, as revealed by extended X-ray absorption fine structure (EXAFS). In general, protons in water molecules located in the first coordination sphere of paramagnetic Mn ions contribute mostly to the T_1 relaxivity (Heffern et al., 2014). As shown in Fig. 3b, the Mn···OH₂ bond is reduced in a pH 5.0 buffer in comparison with that in a pH 7.4 buffer. This bond shrinking increases significantly the T_1 -MRI performance of Mn-LDH nanoparticles because T_1 relaxivity is inversely proportional to R^6 (R is the Mn–proton distance) (Caravan et al., 2009). The variation in Mn···(OH₂)_x coordination (the second peak in Fig. 3b) of Mn-LDH in the pH 5.0 buffer leads to the excellent T_1 -weighted MRI performance of these Mn-LDH nanoparticles in the acidic environment, which has been further demonstrated by in vivo MR imaging. Similarly, the Mn-coordinated water number is also increased in Mn-LDH in pH 5.0 buffer due to more protonation in comparison with that in the pH 7.4 buffer, which enhances linearly the r_1 relaxivity in acidic solution.

The T_1 -MRI performance of Mn-LDH nanoparticles is further used for an in vivo tumor model. Mn-LDH nanoparticles were pre-coated with BSA to prevent aggregation in the physiological environment, as reported by Gu et al. (2015). The resultant BSA/Mn-LDH nanoparticles had an average diameter of $\sim 68 \text{ nm}$ and a zeta potential of $+37.9 \text{ mV}$. The BSA coating did not affect the pH ultrasensitivity of Mn-LDH nanoparticles for MR imaging in the pH range 7.4–6.0.

As shown in Fig. 4a, a remarkable T_1 -weighted signal was observed around the tumor tissue 0.5 h after the intravenous injection of BSA/Mn-LDH nanoparticles. This signal continued to increase in intensity for 24 h, but decreased gradually over the following 2 days (Fig. 4). The time course reveals that BSA/Mn-LDH nanoparticles were accumulated continuously around the tumor tissue, probably due to the ‘enhanced permeability and retention’ (EPR) effect. At the same time, accumulated LDH nanoparticles were metabolized or biodegraded (dissolution in the acidic tumor environment and digestion by tumor cells). Competition between accumulation and biodegradation of BSA/Mn-LDH nanoparticles around the tumor tissue thus explains the T_1 -MRI intensity variations. During the first 24 h post injection, Mn-LDH accumulation was predominant, increasing imaging intensity to reach its zenith at 24 h; afterwards, Mn-LDH biodegradation was quicker than its accumulation, decreasing gradually the imaging brightness until 72 h. This MR imaging profile of BSA/Mn-LDH

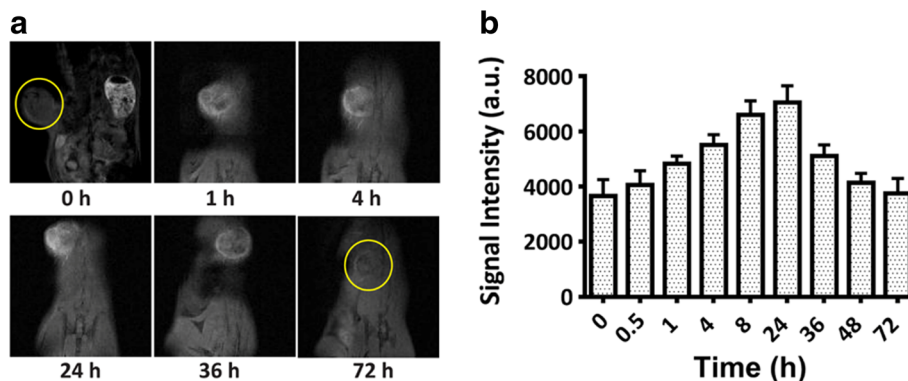


Fig. 4 In vivo MR imaging of BSA/Mn-LDH nanoparticles. A time-course (0, 1, 4, 24, 36, and 72 h) of the contrast enhancement in T_1 -weighted MRI of tumor (a) as well as the corresponding signal intensity variation (b) in the melanoma-tumor-bearing mouse after intravenous injection of BSA/Mn-LDH nanoparticles within 72 h. Error bar = standard deviation, $n = 3$. (Images reproduced with permission from Li et al. 2017)

nanoparticles may diagnose the tumor or other diseased tissues precisely where LDH nanoparticles can be accumulated.

Interestingly, a stronger T_1 -MRI signal was recorded in the tumor compared to that in kidney and liver 24 h post injection, indicating that BSA/Mn-LDH nanoparticles were accumulated selectively in the tumor tissue due to the EPR effect, as supported quantitatively by the amount of Mn accumulated in the tumor tissue, liver, and kidney. Approximately 13.2 ng of Mn ions per mg of tumor, ~ 4.7 ng of Mn ions per mg of kidney, and ~ 3.1 ng of Mn ions per mg of liver were measured. Approximately 3.6% of the injected LDH dose was found to accumulate in the tumor. The effective accumulation of Mn-LDH nanoparticles in the tumor tissue is attributed mainly to the EPR effect. Presumably, the sheet-like morphology may also contribute significantly to this accumulation. Together with the pH-ultrasensitive changes in the tumor microenvironment, Mn-LDH nanoparticles are very promising as an MRI contrast agent for tumor diagnosis.

Replacement of Mg with ^{64}Cu in LDH nanoparticles for PET imaging

BSA-coated Cu-MgAl-LDH (Cu-LDH-BSA) nanoparticles were prepared similarly, i.e. quick precipitation and subsequent hydrothermal treatment to make $\text{Mg}_2\text{Al-CO}_3$ -LDH (Xu et al., 2006a, 2006b; Xu et al., 2008a, 2008b), then coating with BSA, and finally, isomorphic substitution of a very small amount of Mg with ^{64}Cu ions (Shi et al., 2015). As-prepared $\text{Mg}_2\text{Al-CO}_3$ -LDH nanoparticles had an average hydrodynamic diameter of 110 nm. After BSA coating, the average size of the LDH-BSA increased slightly to 130 nm. After the ^{64}Cu isotope was mixed directly with LDH-BSA in a corresponding buffer (referred to as LDH-BSA; chelator-free labeling), the average particle size was said not to change significantly.

^{64}Cu -LDH-BSA nanoparticles in suspension were injected intravenously into 4T1 tumor-bearing mice to examine their in vivo distribution profiles. PET imaging was performed at various time points (0.5, 3, 16, and 24 h post-injection) using a

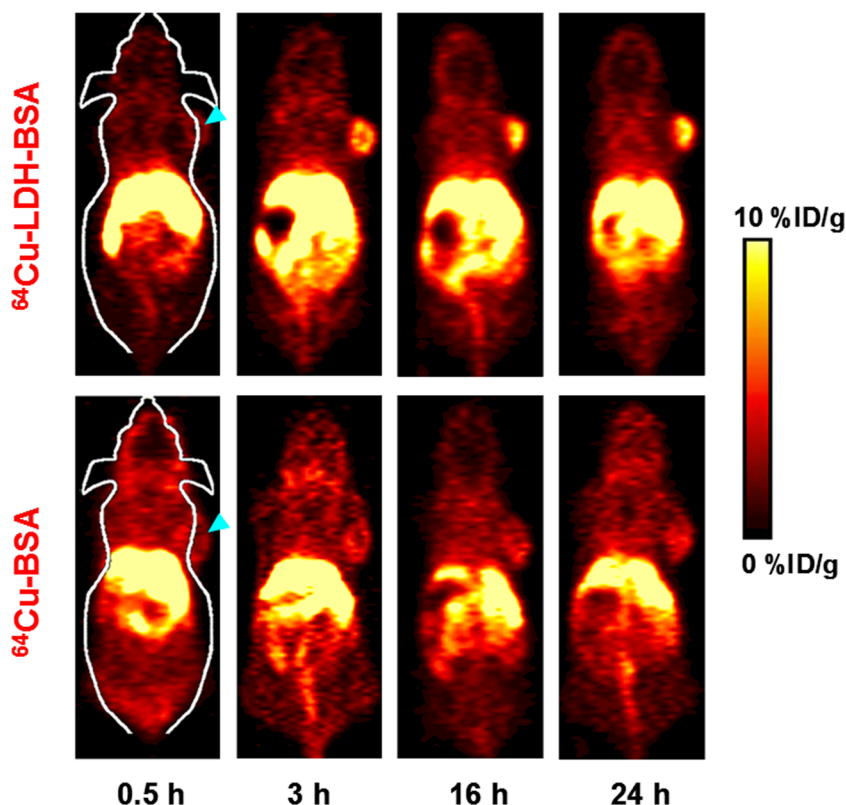
micro-PET/micro-CT Inveon rodent model scanner (Siemens, Suffolk, UK). The coronal PET images (Fig. 5) were treated for quantitative region-of-interest (ROI) analysis (Fig. 6). Prompt and persistent tumor accumulation was achieved via passive targeting, with the accumulated amount being 3.5 ± 1.2 , 7.2 ± 0.5 , 7.7 ± 0.1 , and $6.8 \pm 0.2\%$ ID/g (injected dose per gram) at 0.5, 3, 16, and 24 h post injection, respectively. In contrast, retention in blood and muscle was much less at all time points (Fig. 6a). The tumor/muscle ratios of 4.9 ± 2.0 , 8.9 ± 1.1 , 9.1 ± 1.4 , and 8.6 ± 0.9 were observed at 0.5, 3, 16, and 24 h post injection, respectively (Fig. 6d), suggesting excellent accumulation in the tumor. In comparison, the signal in liver peaked early and decreased quickly with time (Fig. 6a), indicating the hepatic clearance of ^{64}Cu -LDH-BSA nanoparticles.

The PET imaging by intravenous injection of ^{64}Cu -BSA further confirmed the imaging capacity of ^{64}Cu -LDH-BSA for tumor tissues through the passive targeting pathway. As shown in Figs. 5 and 6, significantly less accumulation of molecule-based ^{64}Cu -BSA in the tumors was observed, being relatively unchanged (2.9 ± 0.3 , 3.4 ± 0.1 , 4.1 ± 0.5 , and $4.0 \pm 0.3\%$ ID/g at 0.5, 3, 16, and 24 h post injection). Moreover, the background signal in muscle was relatively stronger (1.9 ± 0.2 , 1.5 ± 0.2 , 1.1 ± 0.1 , and $1.0 \pm 0.1\%$ ID/g at 0.5, 3, 16, and 24 h post injection, respectively; Fig. 6b), possibly due to the much smaller size of ^{64}Cu -BSA compared with ^{64}Cu -LDH-BSA. Both variations led to a poorer imaging contrast, i.e. smaller tumor/muscle ratio (1.5 ± 0.2 , 2.2 ± 0.3 , 3.6 ± 0.5 and 3.8 ± 0.5 at 0.5, 3, 16, and 24 h post injection, respectively; Fig. 6c). Taken together, with a prominent tumor accumulation and excellent imaging-contrast capability, ^{64}Cu -LDH-BSA nanoparticles shows promise as a nanoplatform for in vivo tumor imaging and diagnosis.

COMBINATION THERAPY OF TUMOR CELLS

Many investigations have been carried out using LDH nanoparticles for the effective delivery of a single therapeutic substance, e.g. anti-cancer drugs MTX and 5-FU, the anti-restenotic drug heparin, and siRNA and DNA, have been

Fig. 5 In vivo PET imaging. Serial coronal PET images at different time points post-injection of ^{64}Cu -LDH-BSA and ^{64}Cu -BSA were acquired in 4 T1 tumor-bearing mice. A strong signal in the tumor was observed for the mice injected with ^{64}Cu -LDH-BSA. (Images reproduced with permission (Shi et al., 2015))



summarized previously (e.g. Choy et al., 2004). A more recent strategy is to use LDH nanoparticles to co-load and co-deliver two therapeutic agents in order to synergize the treatment of diseases, such as cancer cells.

The first example is co-delivery of two therapeutic agents (5-FU and functional siRNA) which were co-loaded onto MgAl-LDH nanoparticles using a step-by-step method, as outlined in Fig. 7. First, an homogeneous MgAl-LDH nanoparticle (~100 nm wide) suspension was prepared using the co-precipitation and hydrothermal treatment method (Xu et al., 2006a). Then, 5-FU was intercalated into the MgAl-LDH nanoparticles via the ion-exchange process. 5-FU/LDH hybrid nanoparticles had a similar particle-size distribution with 10% interlayer Cl^- replaced with 5-FU. These hybrid nanoparticles were further loaded with functional siRNA (cell death siRNA) (siRNA-5-FU/LDH), with the average particle diameter unchanged. The value for the mass ratio of siRNA to 5-FU/LDH varied between 1:5 to 1:40, and almost all siRNA was loaded onto the 5-FU/LDH nanoparticle surface.

Firstly, the cytotoxicity of MgAl-LDH nanoparticles for MCF-7 cells in the concentration range of 50–200 $\mu\text{g}/\text{mL}$ was very limited as the cell viability was >90% following a 3-day incubation (Li et al., 2014). Thus, MgAl-LDH nanoparticles can be used safely as a drug- and gene-delivery system. The usual amount of LDH used is <50 $\mu\text{g}/\text{mL}$ is the tests.

The cytotoxicity of 5-FU and 5-FU/LDH for MCF7 cells was examined (Li et al., 2014). As shown in Fig. 7, treatment

with 5-FU reduced the cell viability in a dose-dependent manner and ~45% of MCF-7 cells was killed at 9.6 $\mu\text{g}/\text{mL}$, in agreement with previous reports (Chow & Loo, 2003; Chumakova et al., 2006). Clearly, 5-FU/LDH nanoparticles caused considerably more MCF7 cell death and decreased the cell viability by 20–30% more at each concentration point in the range 0.6–9.6 $\mu\text{g}/\text{mL}$, compared with free 5-FU. This enhancement reflects the more efficient cellular uptake of 5-FU via LDH nanoparticles compared to free 5-FU (Choi et al., 2008), as reported for the cellular uptake of negatively charged FITC (fluorescein isothiocyanate) and dsDNA (double stranded DNA) (Xu et al., 2008b).

Treatment with functional cell death siRNA (CD-siRNA) did not just cause obvious cell death, even at a concentration of 80 nM in the medium, mainly because the negatively charged siRNA cannot be taken up easily by cells. In contrast, when CD-siRNA was loaded onto LDH, ~35% of MCF-7 cells were killed at 40 nM of siRNA in siRNA/LDH nanoparticle form without 5-FU (Fig. 8). The enhanced cytotoxicity further indicated the facilitation of the cellular uptake of negatively charged therapeutics (such as 5-FU and siRNA) via LDH nanoparticles.

Remarkably, co-delivery of CD-siRNA and 5-FU by MgAl-LDH nanoparticles further decreased the cell viability, particularly at the lower 5-FU concentration range (Fig. 8). For example, treatment with CD-siRNA-5-FU/LDH nanoparticles (1.2 $\mu\text{g}/\text{mL}$ of 5-FU and 40 nM of siRNA) killed ~70% of MCF-7 cells, while a single treatment with either 5-FU/LDH or siRNA/LDH at the same

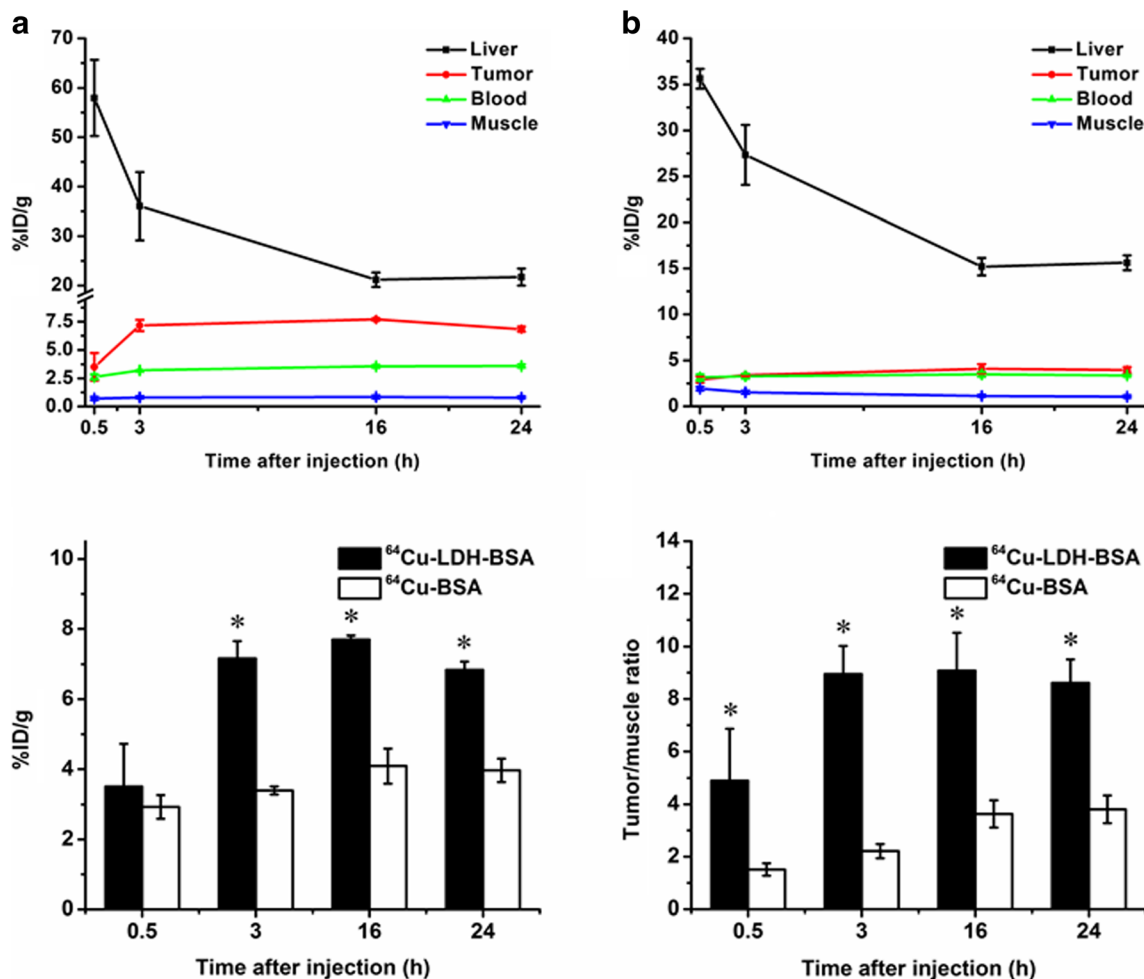


Fig. 6 Quantitative analysis of the PET data: (a) Time activity curves of the liver, 4 T1 tumor, blood, and muscle upon intravenous injection of ^{64}Cu -LDH-BSA. (b) Time activity curves of the liver, 4 T1 tumor, blood, and muscle upon intravenous injection of ^{64}Cu -BSA. (c) Comparison of tumor uptake at various time points post injection of ^{64}Cu -LDH-BSA and ^{64}Cu -BSA. The differences in terms of tumor uptake were statistically significant ($P < 0.05$) at all time points except 0.5 h. (d) Comparison of tumor/muscle ratio at various time points post injection of ^{64}Cu -LDH-BSA and ^{64}Cu -BSA. The differences in tumor/muscle ratio were statistically significant ($P < 0.05$) at all time points. All data represent three mice per group. (Images reproduced with permission, from Shi et al. 2015)

concentration of 5-FU or siRNA only resulted in 46% or 34% of cell death, respectively. Thus, co-delivery of CD-siRNA and 5-FU with MgAl-LDH nanoparticles suppressed MCF-7 cell growth to a significant extent, probably in a synergistic manner. Further analysis shows that the level of anti-apoptosis protein Bcl-2 was reduced

significantly after combination treatment with CD siRNA-5-FU/LDH nanoparticles. The over-expression of Bcl-2 is well known as one of the major mechanisms by which various cancer cells acquire resistance to apoptosis. Thus, the reduction of Bcl-2 expression, induced by siRNA-5-FU/LDH, leads to more cell death.

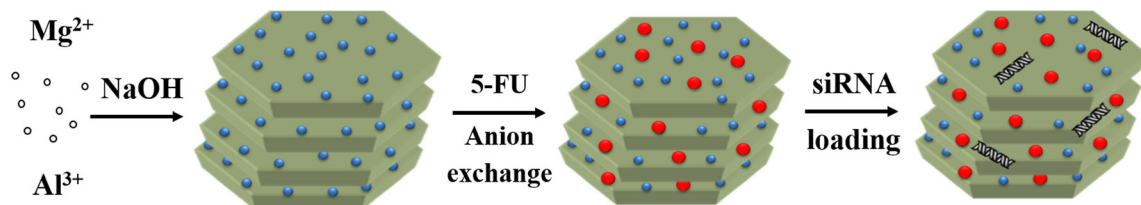


Fig. 7 Schematic illustration for the step-by-step preparation of 5-FU/siRNA-LDH nanoparticles. (Image reproduced with permission, from Li et al. 2014)

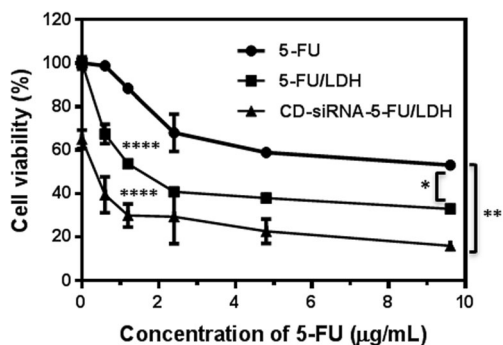


Fig. 8 MTT assay analysis of effects of treatments with 5-FU, 5-FU(10)/LDH, DC-siRNA/LDH, and CD-siRNA-5-FU/LDH on the viability of MCF-7 cells at the 5-FU concentration of 0–9.6 µg/mL and the CD-siRNA concentration at 40 nM in all relevant treatments for 72 h at 37°C. Data represent mean ±SD ($n=5$). *: $p < 0.05$; **: $p < 0.01$; ***: $p < 0.0001$; all vs. 5-FU treatment. (Image reproduced, with permission, from Li et al., 2014)

A co-delivery strategy using MgAl-LDH nanoparticles has been found to be effective for other cancer cell lines, e.g. U2OS and HCT-116. The combination treatment of U2OS or HCT-116 cells with CD-siRNA and 5-FU co-delivered by MgAl-LDH resulted in significant suppression of cell growth compared to a treatment with either CD-siRNA/LDH or 5-FU/LDH alone.

Another example is the use of 5-FU/LDH nanoparticles to treat HCT-116 cells in combination with free BEZ-235, a common drug for treatment of colon cancer. BEZ-235 cannot be loaded onto the LDH nanoparticles, so this combination treatment consisted of 5-FU/LDH nanoparticles and the molecular drug BEZ-235 only.

The growth of the colon cancer cells (HCT-116) was inhibited either by 5-FU/LDH nanoparticles or BEZ-235 in a dose-dependent manner (Chen, Cooper, et al., 2013; Chen, Yee, et al., 2013). The half-maximal inhibitory concentration (IC₅₀) was ~100 nM for BEZ-235 and 6 µg/mL for 5-FU in LDH-5-

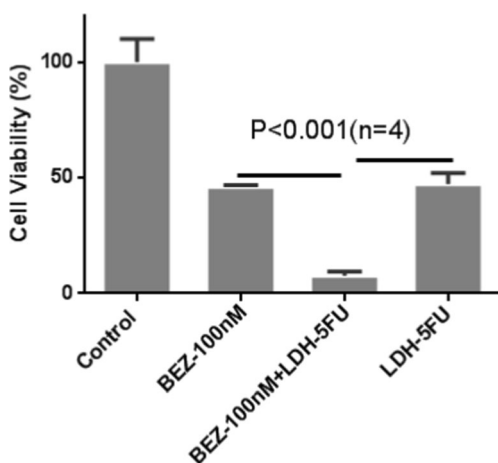


Fig. 9 Combination treatment of colon cancer cells, HCT-116, with BEZ-235 and LDH-5-FU at [BEZ-235] = 100 nM and [5-FU] = 6 µg/mL in LDH-5-FU nanoparticles for 24 h at 37°C. Figure is reproduced, with permission, from Chen et al. 2014)

FU nanoparticles. Combined use of BEZ-235 and LDH-5-FU nanoparticles at both IC₅₀ concentrations resulted in reduction of cell viability to only 8% (Fig. 9). The cell survival rate was significantly less than their linear combination effect ($50\% \times 50\% = 25\%$), indicating their synergistic effect (Ito et al., 2007).

5-FU is a common chemotherapeutic agent used in treatment of colon cancer, and is a suicide inhibitor of thymidylate synthase, an enzyme necessary for DNA replication (Copur et al., 1995; Johnston et al., 1995). The rationale for applying 5-FU and the PI3K/Akt inhibitor BEZ-235 is based on its effective inhibition of the pathway for colon-cancer treatment (Chen, 2011; Manara et al., 2010; Wu & Hu, 2010). Inhibition of the pathway increases the colon cancer cell sensitivity to 5-FU. This is why dual inhibitor BEZ-235 for the PI3K/Akt/mTOR pathway sensitizes HCT-116 cells to LDH-packed 5-FU treatment.

CONCLUSIONS AND EXPERT OPINIONS

Incorporating functional metal cations into the hydroxide layers enables the LDH nanoparticles to be used for efficient imaging of tumor tissue. The signal-change profile in the MRI and PET images reveals clearly that LDH nanoparticles accumulate in the tumor tissue with the maximum level at 24 h post-injection. LDH nanoparticles are able to co-load and co-deliver two therapeutic agents, which inhibit the tumor-cell growth much more efficiently in a synergistic manner. These results show that the LDH nanoparticles can be a simple yet effective theranostic agent.

Incorporation of other functional metal cations, such as Cu, Fe, and Gd, in the hydroxide layer may be possible to make functional LDH nanoparticles for use as pH-sensitive imaging agents. These metal cations may also function as an agent for photothermal therapy. In particular, if the functional metal cations are incorporated into the LDH layers that are fully delaminated, the delivery and imaging capability and the pH sensitivity may be enhanced significantly, as reported by Mei et al. (2018a, 2018b). Predictably, LDH nanoparticles will be tested for co-delivery of two or more negatively charged antitumor therapeutic agents for efficient inhibition of tumor-cell growth in animal models. A more ambitious prediction is to combine the imaging capability and therapeutic efficacy, together with the efficient passive targeting of plate-like LDH nanoparticles for tumor tissue, to allow for simultaneous imaging and treatment of the tumor in vivo.

ACKNOWLEDGMENTS

This work was supported financially by an Australian Research Council (ARC) grant (DP170104643) and the Australian Government Research Training Program Scholarship (RTP). The authors acknowledge the facilities and the assistance of Queensland Node of the Australian National Fabrication Facility (ANFF-Q), the University of Queensland.

REFERENCES

- Caravan, P., Farrar, C. T., Frullano, L., & Uppal, R. (2009). Influence of molecular parameters and increasing magnetic field strength on relaxivity of gadolinium- and manganese-based T1 contrast agents. *Contrast Media & Molecular Imaging*, 4, 89–100.
- Chen, C., Yee, L. K., Gong, H., Zhang, Y., & Xu, R. (2013). A facile synthesis of strong near infrared fluorescent layered double hydroxide nanovehicles with an anticancer drug for tumor optical imaging and therapy. *Nanoscale*, 5, 4314–4320.
- Chen, J. (2011). Multiple signal pathways in obesity-associated cancer. *Obesity Reviews*, 12, 1063–1070.
- Chen, J. Z., Shao, R. F., Li, L., Xu, Z. P., & Gu, W. Y. (2014). Effective inhibition of colon cancer cell growth with MgAl-layered double hydroxide (LDH) loaded 5-FU and PI3K/mTOR dual inhibitor BEZ-235 through apoptotic pathways. *International Journal of Nanomedicine*, 9, 3403–3411.
- Chen, M., Cooper, H. M., Zhou, J. Z., Bartlett, P. F., & Xu, Z. P. (2013). Reduction in the size of layered double hydroxide nanoparticles enhances the efficiency of siRNA delivery. *Journal of Colloid And Interface Science*, 390, 275–281.
- Choi, G., Piao, H., Alotman, Z. A., Vinu, A., Yun, C. O., & Choy, J. H. (2016). Anionic clay as the drug delivery vehicle: tumor targeting function of layered double hydroxide-methotrexate nanohybrid in C33A orthotopic cervical cancer model. *International Journal of Nanomedicine*, 11, 337–348.
- Choi, S. J., Oh, J. M., & Choy, J. H. (2008). Anticancer drug-layered hydroxide nanohybrids as potent cancer chemotherapy agents. *Journal of Physics and Chemistry of Solids*, 69, 1528–1532.
- Choi, S. J., & Choy, J. H. (2011). Layered double hydroxide nanoparticles as target-specific delivery carriers: uptake mechanism and toxicity. *Nanomedicine*, 6, 803–814.
- Chow, L. W. C., & Loo, W. T. Y. (2003). The differential effects of cyclophosphamide, epirubicin and 5-fluorouracil on apoptotic marker (CPP-32), proapoptotic protein (p21WAF-1) and anti-apoptotic protein (bcl-2) in breast cancer cells. *Breast Cancer Research Treatment*, 80, 239–244.
- Choy, J. H., Jung, J. S., Oh, J. M., Park, M., Jeong, J., Kang, Y. K., & Han, O. J. (2004). Layered double hydroxide as an efficient drug reservoir for folate derivatives. *Biomaterials*, 25, 3059–3064.
- Chumakova, O. V., Liopo, A. V., Mark, E. B., & Esenaliev, R. O. (2006). Effect of 5-fluorouracil, optison and ultrasound on MCF-7 cell viability. *Ultrasound in Medicine and Biology*, 32, 751–758.
- Copur, S., Aiba, K., Drake, J. C., Allegra, C. J., & Chu, E. (1995). Thymidylate synthase gene amplification in human colon cancer cell lines resistant to 5-fluorouracil. *Biochemical Pharmacology*, 49, 1419–1426.
- Desigaux, L., Richard, P., Pitard, B., Belkacem, M. B., Cellier, J., Leroux, F., Tavio-Guêho, C., Léone, P., & Cario, L. (2006). Self-assembly and characterization of layered double hydroxide/DNA hybrids. *Nano Letters*, 6, 199–204.
- Donahue, K. M., Burstein, D., Manning, W. J., & Gray, M. L. (1994). Studies of Gd-DTPA relaxivity and proton exchange rates in tissue. *Magnetic Resonance in Medicine*, 32, 66–76.
- Gu, Z., Zuo, H. L., Li, L., Wu, A. H., & Xu, Z. P. (2015). Pre-coating layered double hydroxide nanoparticles with albumin to improve colloidal stability and cellular uptake. *Journal of Materials Chemistry B*, 3, 3331–3339.
- Heffern, M. C., Matosziuk, L. M., & Meade, M. J. (2014). Lanthanide probes for bioresponsive imaging. *Chemical Reviews*, 114, 4496–4539.
- Ito, A., Fujioka, M., Yoshida, T., Wakamatsu, K., Ito, S., Yamashita, T., Jimbow, K., & Honda, H. (2007). 4-S-cysteaminylphenol-loaded magnetite cationic liposomes for combination therapy of hyperthermia with chemotherapy against malignant melanoma. *Cancer Science*, 98, 424–430.
- Johnston, P. G., Lenz, H. J., Leichman, C. G., Danenberg, K. D., Allegra, C. J., Danenberg, P. V., & Leichman, L. (1995). Thymidylate synthase gene and protein expression correlate and are associated with response to 5-fluorouracil in human colorectal and gastric tumors. *Cancer Research*, 55, 1407–1412.
- Khan, A. I., Lei, L., Norquist, A. J., & Hare, D. (2001). Intercalation and controlled release of pharmaceutically active compounds from a layered double hydroxide. *Chemical Communications*, 0, 2342–2343.
- Lee, J. H., Jung, D. Y., Kim, E., & Ahn, T. K. (2014). Fluorescein dye intercalated layered double hydroxides for chemically stabilized photoluminescent indicators on inorganic surfaces. *Dalton Transactions*, 43, 8543–8548.
- Li, B., Gu, Z., Kurniawan, N., Chen, W. Y., & Xu, Z. P. (2017). Manganese-based layered double hydroxide nanoparticle as a T1-MRI contrast agent with ultrasensitive pH response and high relaxivity. *Advanced Materials*, 29, 1700373.
- Li, D., Zhang, Y. T., Yu, M., Guo, J., Chaudhary, D., & Wang, C. C. (2013). Cancer therapy and fluorescence imaging using the active release of doxorubicin from MSPs/Ni-LDH folate targeting nanoparticles. *Biomaterials*, 34, 7913–7922.
- Li, L., Gu, W., Chen, J., Chen, W., & Xu, Z. P. (2014). Co-delivery of siRNAs and anti-cancer drugs using layered double hydroxide nanoparticles. *Biomaterials*, 35, 3331–3339.
- Li, L., Gu, W., Liu, J., & Xu, Z. P. (2015). Amine-functionalized SiO₂ nanodot-coated layered double hydroxide nanocomposites for enhanced gene delivery. *Nano Research*, 8, 682–694.
- Li, X. S., Ke, M. R., Huang, W., Ye, C. H., & Huang, J. D. (2015). A pH-responsive layered double hydroxide (LDH)-phthalocyanine nanohybrid for efficient photodynamic therapy. *Chemistry - A European Journal*, 21, 3310–3317.
- Manara, M. C., Nicoletti, G., Zambelli, D., Ventura, S., Guerzoni, C., Landuzzi, L., Lollini, P. L., Maira, S. M., García-Echeverría, C., Mercuri, M., Picci, P., & Scotlandi, K. (2010). NVP-BEZ235 as a new therapeutic option for sarcomas. *Clinical Cancer Research*, 16, 530–540.
- Mei, X., Ma, J., Bai, X., Zhang, X., Zhang, S., Liang, R., Wei, M., Evans, D. G., & Duan, X. (2018a). A bottom-up synthesis of rare-earth-hydroxalite monolayer nanosheets toward multimode imaging and synergetic therapy. *Chemical Science*, 9, 5630–5639.
- Mei, X., Wang, W., Yan, L., Hu, T., Liang, R., Yan, D., Wei, M., Evans, D. G., & Duan, X. (2018b). Hydroxalite monolayer toward high performance synergistic dual-modal imaging and cancer therapy. *Biomaterials*, 165, 14–24.
- Park, A.-Y., Kwon, H., Woo, A. J., & Kim, S. J. (2005). Layered double hydroxide surface modified with (3-aminopropyl)-triethoxysilane by covalent bonding. *Advanced Materials*, 17, 106–109.
- Shi, S. X., Fliss, B., Gu, Z., Zhu, Y., Hong, H., Valdovinos, H. F., Hernandez, R., Goel, S., Luo, H. M., Chen, F., Barnhart, T. E., Nickles, R. J., Xu, Z. P., & Cai, W. B. (2015). Chelator-free labeling of layered double hydroxide nanoparticles for *in vivo* PET imaging. *Scientific Reports*, 5(16930), 1–10.
- Wang, L., Xing, H. Y., Zhang, S. J., Ren, Q. G., Pan, L. M., Zhang, K., Bu, W. B., Zheng, X. P., Zhou, L. P., Peng, W. J., Hua, Y. Q., & Shi, J. L. (2013). A Gd-doped Mg-Al-LDH/Au nanocomposite for CT/MR bimodal imagings and simultaneous drug delivery. *Biomaterials*, 34, 3390–3401.
- Wang, Q., & O'Hare, D. (2012). Recent advances in the synthesis and application of layered double hydroxide (LDH) nanosheets. *Chemical Reviews*, 112, 4124–4155.
- Wong, Y., Cooper, H. M., Zhang, K., Chen, M., Bartlett, P., & Xu, Z. P. (2012). Efficiency of layered double hydroxide nanoparticle-mediated delivery of siRNA is determined by nucleotide sequence. *Journal of Colloid And Interface Science*, 369, 453–459.
- Wu, P., & Hu, Y. Z. (2010). PI3K/Akt/mTOR pathway inhibitors in cancer: a perspective on clinical progress. *Current Medicinal Chemistry*, 17, 4326–4341.
- Xu, Z. P., & Lu, G. Q. (2005). Hydrothermal synthesis of layered double hydroxides (LDHs) from mixed MgO and Al₂O₃: LDH formation mechanism. *Chemistry of Materials*, 17, 1055–1062.
- Xu, Z. P., Stevenson, G. S., Lu, C. Q., & Lu, G. Q. (2006a). Dispersion and size control of layered double hydroxide nanoparticles in

- aqueous solutions. *The Journal of Physical Chemistry B*, 110, 16923–16929.
- Xu, Z. P., Stevenson, G. S., Lu, C. Q., Lu, G. Q., Bartlett, P. F., & Gray, P. P. (2006b). Stable suspension of layered double hydroxide nanoparticles in aqueous solution. *Journal of the American Chemical Society*, 128, 36–37.
- Xu, Z. P., Jin, Y. G., Liu, S. M., Hao, Z. P., & Lu, G. Q. (2008a). Surface charging of layered double hydroxides during dynamic interactions of anions at the interfaces. *Journal of Colloid And Interface Science*, 326, 522–529.
- Xu, Z. P., Niebert, M., Porazik, K., Walker, T. L., Cooper, H. M., Middelberg, A. P. J., Gray, P. P., Bartlett, P. F., & Lu, G. Q. (2008b). Subcellular compartment targeting of layered double hydroxide nanoparticles. *Journal of Controlled Release*, 130, 86–94.
- Zuo, H. L., Chen, W., Li, B., Xu, K., Cooper, H., Gu, Z., & Xu, Z. P. (2017). MnAl- layered double hydroxide nanoparticles as a dual-functional platform for magnetic resonance imaging and siRNA delivery. *Chemistry – A European Journal*, 23, 14299–14306.

[Received 28 April 2018; revised 23 August 2018; AE: J.-H. Choy]